Parker Solar Probe In Situ Observations of Magnetic Reconnection Exhausts during Encounter 1

T. D. Phan[1], S. D. Bale[1,2,3], J. P. Eastwood[3], B. Lavraud[4], J. F. Drake[5], M. Oieroset[1], M. A. Shay[6], M. Pulupa[1],
M. Stevens[7], R. J. MacDowall[8], A. W. Case[7], D. Larson[1], J. Kasper[9], P. Whittlesey[1], A. Szabo[8], K. E. Korreck[7],
J. W. Bonnell[1], T. Dudok de Wit[10], K. Goetz[11], P. R. Harvey[1], T. S. Horbury[3], R. Livi[1], D. Malaspina[12], K. Paulson[7],
N. E. Raouafi[13], and M. Velli[14]

[1] SSL, University of California, Berkeley, CA 94720, USA; phan@ssl.berkeley.edu
[2] Physics Department, University of California, Berkeley, CA 94720-7300, USA
[3] The Blackett Laboratory, Imperial College London, London, UK
[4] IRAP, Université de Toulouse, France
[5] University of Maryland, College Park, MD, USA
[6] University of Delaware, Newark, DE, USA
[7] Smithsonian Astrophysical Observatory, Cambridge, MA, USA
[8] NASA Goddard Space Flight Center, Greenbelt, MD, USA
[9] Climate and Space Sciences and Engineering, University of Michigan, Ann Arbor, MI, USA
[10] LPC2E, CNRS and University of Orléans, Orléans, France
[11] School of Physics and Astronomy, University of Minnesota, Minneapolis, MN, USA
[12] University of Colorado LASP, Boulder, CO, USA
[13] Johns Hopkins University Applied Physics Laboratory, Laurel, MD, USA
[14] University of California, Los Angeles, Los Angeles, CA, USA

Abstract

Magnetic reconnection in current sheets converts magnetic energy into particle energy. The process may play an important role in the acceleration and heating of the solar wind close to the Sun. Observations from *Parker Solar Probe* (*PSP*) provide a new opportunity to study this problem, as it measures the solar wind at unprecedented close distances to the Sun. During the first orbit, *PSP* encountered a large number of current sheets in the solar wind through perihelion at 35.7 solar radii. We performed a comprehensive survey of these current sheets and found evidence for 21 reconnection exhausts. These exhausts were observed in heliospheric current sheets, coronal mass ejections, and regular solar wind. However, we find that the majority of current sheets encountered around perihelion, where the magnetic field was strongest and plasma β was lowest, were Alfvénic structures associated with bursty radial jets, and these current sheets did not appear to be undergoing local reconnection. We examined conditions around current sheets to address why some current sheets reconnected while others did not. A key difference appears to be the degree of plasma velocity shear across the current sheets: the median velocity shear for the 21 reconnection exhausts was 24% of the Alfvén velocity shear, whereas the median shear across 43 Alfvénic current sheets examined was 71% of the Alfvén velocity shear. This finding could suggest that large, albeit sub-Alfvénic, velocity shears suppress reconnection. An alternative interpretation is that the Alfvénic current sheets are isolated rotational discontinuities that do not undergo local reconnection.

Unified Astronomy Thesaurus concepts: Space plasmas (1544); Plasma astrophysics (1261); Solar magnetic reconnection (1504); Solar magnetic fields (1503); Alfven waves (23); Solar wind (1534)

1. Introduction

Magnetic reconnection in current sheets is a universal plasma process that converts magnetic energy into plasma jetting and heating and is important in many laboratory, space, solar, and astrophysical contexts (e.g., Parker 1983; Priest 1984; Duncan & Thompson 1992; Kronberg 2002; Hurley et al. 2005; Yamada 2010; Abdo et al. 2011, Paschmann et al. 2013a). For example, reconnection plays an important role transferring solar wind mass, momentum, and energy into the magnetosphere of Earth (e.g., Dungey 1961) and other planets (e.g., Slavin & Holzer 1979). On the Sun, it has been suggested that reconnection plays an important role in the heating of the corona (e.g., Parker 1988; Klimchuk 2006) and initiation of solar flares (e.g., Giovanelli 1946; Parker 1963; Antiochos et al. 1999), as well as the restructuring of the corona over the solar cycle (e.g., Babcock 1961; Leighton 1969; Owens et al. 2007; Lavraud et al. 2011). In the solar wind, in situ observations by spacecraft at 1 au and beyond have revealed the presence of reconnection exhausts in

current sheets in the vicinity of interplanetary coronal mass ejections (ICMEs; e.g., Gosling et al. 2007; Gosling & Szabo 2008; Phan et al. 2009; Ruffenach et al. 2012, 2015; Lavraud et al. 2014), at heliospheric current sheets (HCSs; e.g., Gosling et al. 2005b, 2006a; Lavraud et al. 2009), and in the regular solar wind (e.g., Gosling et al. 2005a, 2006b; Davis et al. 2006; Phan et al. 2006, 2010; Gosling 2007; Eriksson et al. 2009; Mistry et al. 2015, 2017).

At 1 au, reconnection is detected in only a small fraction of the solar wind current sheets encountered by spacecraft; thus, reconnection is not energetically important at 1 au in terms of the evolution of heliospheric plasmas and fields (Gosling et al. 2005a, 2007). However, it is predicted that the occurrence rate of reconnection in solar wind current sheets could be much higher closer to the Sun because of the lower plasma β environment there, which lessens constraints on the occurrence of reconnection associated with the magnetic geometry of the current sheet (Swisdak et al. 2003, 2010; Phan et al. 2010).
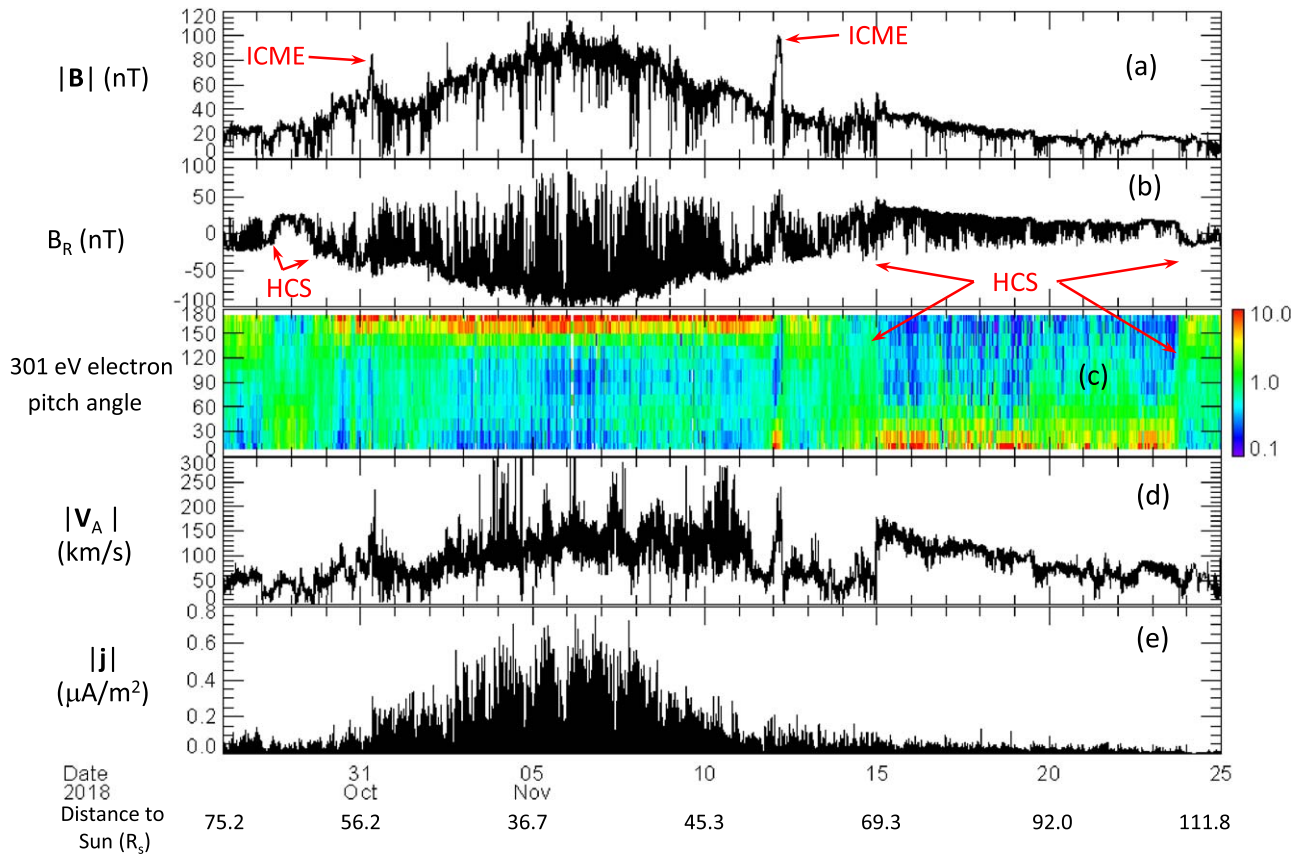
Figure 1. Overview of encounter 1 showing (1) current density spikes indicative of the presence of a large number of current sheets throughout the encounter and (2) the locations of HCSs and ICMEs where reconnection exhausts are seen. (a) Magnetic field magnitude, (b) radial component of the magnetic field, (c) normalized pitch angle energy fluxes of 310 eV (strahl) electrons measured by SWEAP/SPAN, (d) Alfvén speed, and (e) proxy for current density, $|j| = [(\delta B_R/\delta t)^2 + (\delta B_T/dt)^2 + (\delta B_N/dt)^2)]^{1/2}/(\mu_0 V_{pR})$, where V_{pR} is the radial component of the proton velocity.

Parker Solar Probe (*PSP*; Fox & McComas 2016) provides an unprecedented opportunity to probe the physics and properties of solar wind reconnection in the near-Sun environment. During the first orbit, *PSP*'s closest approach was 35.7 solar radii (R_s), allowing reconnection to be explored at such close distances to the Sun for the first time. We have performed a comprehensive survey of plasma and field measurements to determine the occurrence of reconnection exhausts, providing a first assessment of the role reconnection might play in the solar wind close to the Sun. We present examples of reconnection exhausts in and around an ICME, HCS crossings, and the regular solar wind. We find no evidence of reconnection near orbit 1 perihelion; at this time, the solar wind appeared to be dominated by Alfvénic structures, rather than reconnection in the local current sheets. Whether the absence of reconnection near perihelion in this orbit is due to the particular type of solar wind encountered or is intrinsic to the near-Sun environment remains to be understood.

The paper is organized as follows. Section 2 describes the data set and methodology used. In Section 3 we show an overview of encounter 1. In Section 4 examples of reconnection exhausts in different environments are presented. We find that the subsecond-resolution plasma and field measurements are often required to resolve thin current sheets encountered during orbit 1. Section 5 shows that plasma jets seen near perihelion are mostly associated with Alfvénic structures, rather than reconnection in the local current sheets. Section 6 discusses statistical properties of current sheets associated with reconnection versus Alfvénic structures. Section 7 summarizes and discusses our findings.

2. Instrumentation, Event Selection Criteria, and Current Sheet Coordinate System

2.1. Instrumentation

We have examined *PSP* data from 2018 October 27 to November 25, covering radial solar distances of 75.2–35.7 R_s on the inbound and up to 111.8 R_s on the outbound legs of orbit 1 (Figure 1). Magnetic field data are measured by the FIELDS fluxgate magnetometer (Bale et al. 2016). The sampling rate of magnetic field data was 290 vectors s^{-1} near perihelion and gradually lower at larger radial distances, with a cadence of 0.2 s at 111 R_s. For uniformity of data presentation and the comparison of current density values at various radial distances (Figure 1(e)), the magnetic field data presented in the present paper have been averaged to 0.2 s.

The proton velocity and density used in this paper are measured by the SWEAP/SPC instrument (Kasper et al. 2016; Case et al. 2020). Here we use the best-resolution data available, which were 0.22 s cadence just prior to the central perihelion pass (2018 November 1/15:28 to 2018 November 3/11:51 UT) and 0.9 s in the intervals on either side (2018 October 31/03:00 to 2018 November 1/15:28 UT before, 2018 November 3/11:51 to 2018 November 11/03:28 UT after). Outside of these times, the SPC proton moment cadence was ~28 s. Electron pitch angle fluxes are measured by the SWEAP/SPAN instrument (Whittlesey et al. 2019). The SWEAP/SPAN electron pitch angle data we use have a cadence of 28 s from 2018 October 31/03:00 UT to 2018

November 12/03:30 UT. The cadence was 900 s outside this interval.

2.2. Reconnection and Nonreconnection Event Identification

We identify reconnection exhausts in current sheets by the presence of accelerated plasma flows. These flows are bounded on one edge of the current sheet by correlated changes in velocity, V, and magnetic field, B, and anticorrelated changes in V and B on the other edge, indicating a pair of rotational discontinuities (RDs) bounding the exhaust. Such opposite correlations between the changes in V and B are consistent with Alfvénic disturbances propagating in opposite directions along reconnected field lines away from the reconnection site (X-line; e.g., Gosling et al. 2005a). We do not identify reconnection events based on magnetic field profiles such as deep minima in $|B|$ or bifurcated current sheets alone, as they are not unique to reconnection events. This means that events can only be identified if their duration is longer than the cadence of the plasma measurements. Examples of reconnection events illustrating the method are shown in Figures 2–4.

In contrast, nonreconnecting current sheets are recognized by the absence of plasma jetting within the current sheets. In such cases, the current sheet could be a tangential discontinuity (TD) or a single RD. Across a TD, the V and B variations are usually not correlated, since the plasmas on the two sides of a TD are not magnetically connected with each other. Across a single RD, there should be a single correlation between V and B. Examples of nonreconnecting current sheets are shown in Figure 5.

2.3. Current Sheet (XYZ) Coordinate System

In the present paper, the data are shown in two coordinate systems. The large-scale context data are shown in the spacecraft-centered RTN coordinate system (Hapgood 1992), where R is the direction from the Sun to the spacecraft, T is the cross product of the Sun's rotation vector with R, and $N = R \times T$. Individual current sheets are shown in a local current sheet (XYZ) coordinate system. This uses a hybrid minimum variance method, which has been found to work well in low magnetic shear (large guide field) current sheets (Gosling & Phan 2013). The current sheet normal direction, Z, is determined from $B_1 \times B_2/|B_1 \times B_2|$, where B_1 and B_2 are the magnetic field vectors at the two edges of the current sheet. Here $Y = Z \times X'$ is approximately the out-of-plane X-line direction, where X' is the maximum variance direction from the minimum variance of the magnetic field (MVAB) analysis (Sonnerup & Cahill 1967), and $X = Y \times Z$ is approximately along the antiparallel magnetic field direction.

3. Overview of Encounter 1

Figure 1 shows the large-scale context of the PSP in situ observations of the solar wind from 2018 October 27 to November 25, with magnetic field magnitude (panel (a)) increasing with decreasing distance to the Sun, reaching $\sim$100 nT near perihelion (see Bale et al. 2019 for details on the radial dependence of the field magnitude). Large fluctuations in the radial component of the magnetic field (panel (b)) are seen throughout the encounter. Figure 1(e) reveals these fluctuations to be associated with current density spikes, reaching $|j|$ $\sim 0.6\,\mu\mathrm{A\,m^{-2}}$ near perihelion on November 5–8. Such peak current densities across magnetic field variations δB up to 100 nT imply current sheet widths ($w \sim \Delta B/\mu_0 j$) of the order of 100 km, compared to the ion inertial length of $\sim$15 km in this

interval. Closer inspection of the current density and magnetic field variations throughout the interval in Figure 1 reveals a range of current sheet thicknesses, from kinetic to MHD scales.

The reconnection exhaust jet speed is expected to scale as the inflow Alfvén speed, and the ambient solar wind Alfvén speed reached an average level of $\sim$150 km s^{-1} near perihelion at 35.7 R_S (around 2019 November 6), more than a factor of 3 larger than at 110 R_s (Figure 1(d)). This indicates that reconnection exhausts, if present, should be easily identifiable in the data.

To set the context for the reconnection exhausts and Alfvénic structures to be described in the next section, certain key regions in which reconnection was detected are labeled in Figures 1(a)–(c). The HCS crossings are recognized by polarity reversals of the large-scale radial magnetic field (Figure 1(b); Bale et al. 2019; Szabo et al. 2020), together with the concurrent switching between 0° and 180° pitch angle of fluxes of 320 eV electrons, which are strahl electrons of solar origin. Two ICMEs encountered by PSP during orbit 1 (Korreck et al. 2019) are also marked in Figure 1(a).

4. Observations of Reconnection Exhausts

We examined the entire 29 day interval shown in Figure 1 to search for evidence for reconnection exhausts. Table 1 lists all 21 reconnection exhausts that we have been able to identify so far in orbit 1, as well as their properties in terms of exhaust width, magnetic and velocity shear values, and the locations and regions in which they were detected. We now show some of the cleanest examples of exhausts detected by PSP, organized by the event environments.

4.1. Reconnection in ICMEs

There were two prominent ICMEs detected by PSP during orbit 1 (Figure 1(a)). The October 31 ICME is smaller than that on November 11–12 (in terms of spatial dimension and magnetic field strength enhancement), but it has the advantage that high time resolution (0.9 s) proton moment data are available.

Figures 2(a) and (b) show the large-scale structure of the October 31 ICME, detected at $\sim$55 R_s as the structure moved past PSP, with a large enhancement in the magnetic field magnitude $|B|$ up to 80 nT. Large rotations of the magnetic field are seen inside the ICME between 08:15 and 08:30 UT on 2018 October 31, although small changes in the magnetic field exist throughout. We found three occurrences of reconnection in current sheets within the ICME. Interestingly, only one of these occurred in a large rotation of the magnetic field, while the other two had extremely small magnetic field rotations. We now describe the three events in detail. The data are presented in the XYZ current sheet coordinate system (see Section 2).

Figures 2(c)–(g) show an event where PSP detected the passage of a current sheet (panel (d)), with an embedded reconnection outflow at 06:43:21–06:43:27 UT (between the two vertical dashed lines). The current sheet crossing duration was only 5.7 s. The exhaust was identified by the presence of accelerated flow in the positive X direction (panel (f)) within the region where the magnetic field rotated (panel (d)), with the change in proton velocity in the outflow direction V_{pX} (panel (f)) and the reconnecting field component B_X (panel (e)) being correlated on the leading edge and anticorrelated on the trailing edge of the exhaust, as described in Section 2. The observed
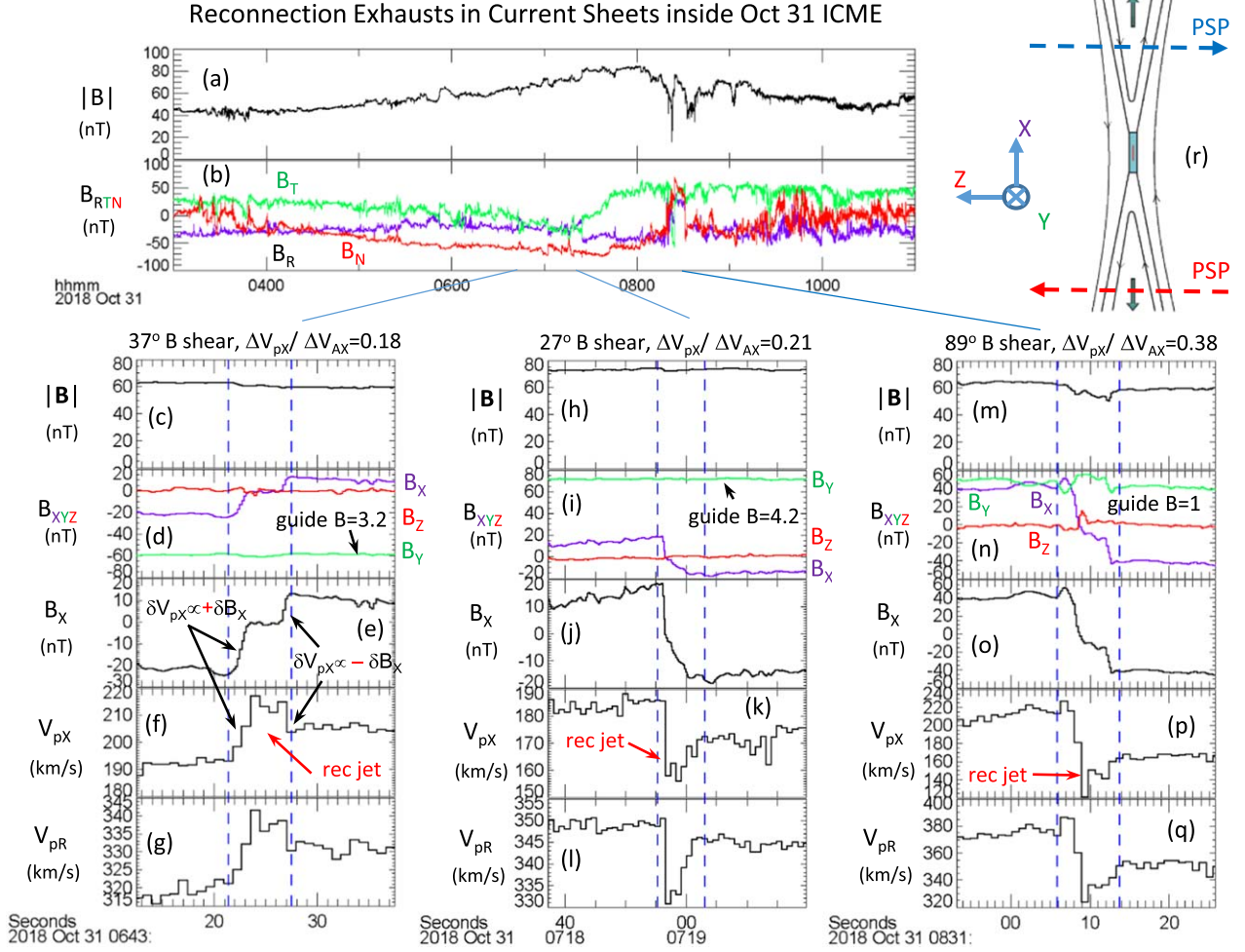
Figure 2. Examples of reconnection exhausts in current sheets associated with an ICME. Panels (a) and (b) show an overview of the ICME on 2018 October 31. Panels (c)–(g) and (h)–(l) are two extremely low magnetic shear current sheets inside the ICME displaying reconnection ion jets. Panels (m)–(q) show the reconnecting current sheet at the compressed trailing edge of the ICME. (a) and (b) Magnetic field magnitude and components in RTN coordinates. (c), (h), (m) Magnetic field magnitude. (d), (i), (n) Magnetic field components in *XYZ* current sheet boundary normal coordinates. (e), (j), (o) *X* component of the magnetic field. (f), (k), (p) *X* component of the proton bulk velocity measured by SWEAP/SPC. (g), (l), (q) *R* component of the proton velocity. (r) Schematic illustrations of reconnection configuration and *PSP* trajectories across a reconnecting sheet above (+*X*) and below (−*X*) the reconnection site. Vertical blue dashed lines approximately mark the two edges of a current sheet where the external conditions have stabilized. The magnetic field and ion velocity values at these two locations are used to compute the magnetic shear angle θ and velocity shear across the current sheet ΔV_{pX}. Panels (e) and (f) show how reconnection exhausts are recognized: correlated changes in V_{pX} and B_X at one edge of a current sheet and anticorrelated changes in V_{pX} and B_X at the other edge, indicative of Alfvén waves propagating in opposite directions along reconnected field lines away from the reconnection *X*-line (e.g., Gosling et al. 2005a).

changes in the outflow velocity V_{px} were $\sim$24 and $\sim$12 km s^{-1} across the leading and trailing edges of the exhaust (going from outside to the middle of the current sheet), respectively, and these changes were $\sim$64% and 59% of the predicted changes at the corresponding edges of the exhaust according to the RD jump condition (Hudson 1970),

$$V_{pX2} - V_{pX1} \sim \pm(B_{X2} - B_{X1})/(\mu_0 \rho_1)^{1/2}, \qquad (1)$$

where V_{pX} and B_X are the X component of the proton bulk velocity and magnetic field, and ρ is the proton mass density (here we omit the pressure anisotropy effect for simplicity). Subscripts 1 and 2 denote the inflow and outflow regions, respectively. The positive and negative signs of this relation refer to the leading and trailing edges of the exhaust, respectively, for this example. The sub-Alfvénic outflow is a common feature of reconnection in observations (e.g., Sonnerup et al. 1981; Paschmann et al. 1986; Øieroset et al. 2000) and kinetic simulations (e.g., Liu et al. 2012;

Haggerty et al. 2018) and has been attributed to the fact that the exhaust boundaries are not pure RDs but rather a combination of RDs and slow shocks (e.g., Lin & Lee 1993; Teh et al. 2009; Liu et al. 2012). It could also be due to the effect of ion temperature anisotropy in the exhaust (Haggerty et al. 2018).

In this event, the reconnection outflow detected by *PSP* was radially anti-sunward, leading to an enhancement of the radial flow speed relative to the ambient solar wind flow (Figure 2(g)). This implies that the *X*-line was located sunward of *PSP*.

The magnetic shear angle (θ) across the current sheet was only $\sim$37°; i.e., the guide field B_Y was 3.2 times the reconnecting field B_X. A characteristic of strong guide field current sheets is that $|\boldsymbol{B}|$ is typically only very slightly depressed inside the reconnecting current sheet, as observed here (see also Gosling & Szabo 2008; Phan et al. 2010), because the guide field is modestly compressed within the exhaust to maintain total pressure balance (Lin & Lee 1993; Zhang et al. 2019). The sharp changes in the magnetic field orientation near the two edges and a plateau in
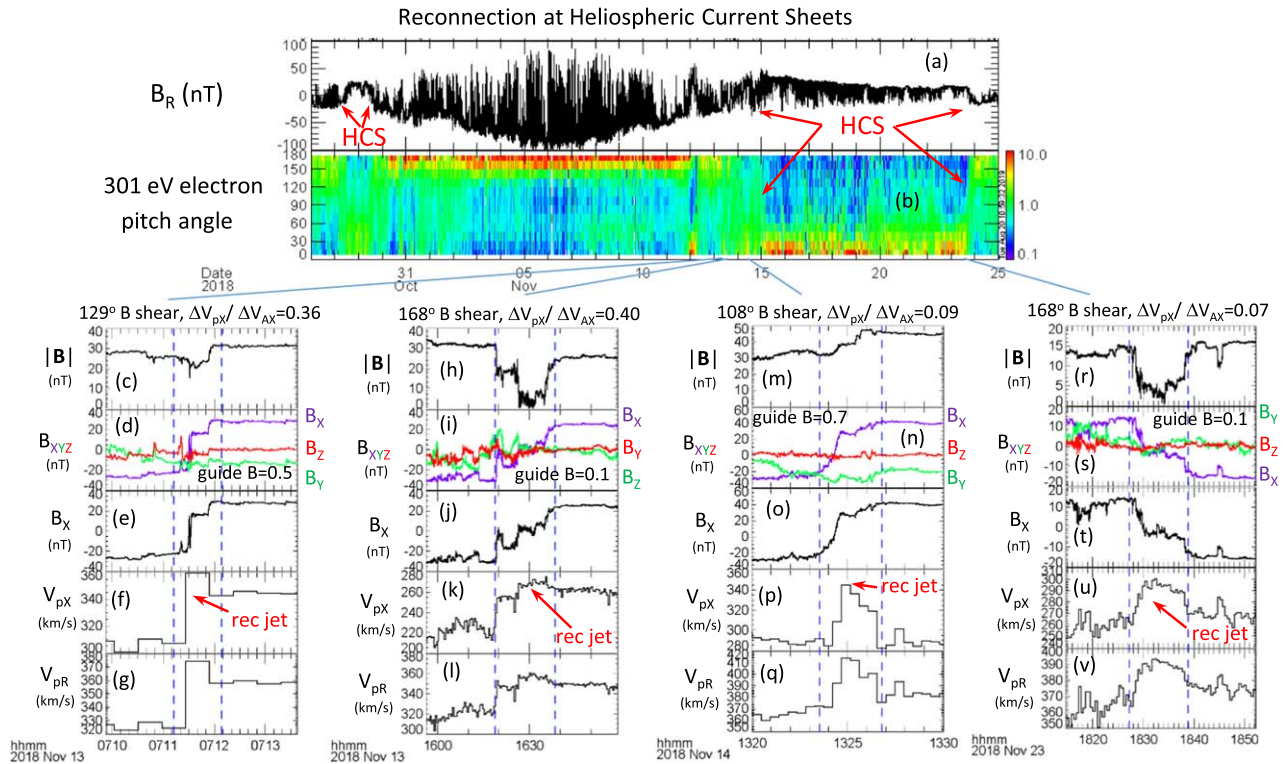
Figure 3. Examples of reconnection exhausts at HCSs. (a) Radial component of the magnetic field. (b) Normalized pitch angle energy fluxes of 310 eV (strahl) electrons. The parameters in panels (c)–(v) are the same as those in Figure 2. Here V_{pR} was positively enhanced in all four current sheets, indicating that the reconnection X-line was sunward of *PSP* in these events.

between indicate that the current sheet was bifurcated (e.g., Phan et al. 2006; Gosling & Szabo 2008). The B_X level of the plateau being above the halfway point between the two asymptotic B_X is due to the presence of tangential V_{pX} velocity shear (Eriksson et al. 2009), such that the jumps in V_{pX} and B_X are larger at the leading edge of the exhaust.

Finally, it is noted that the shear of the velocity component along the reconnecting field direction, ΔV_{pX}, measured by the difference between V_{pX} at the two dashed lines (Figure 2(f)), was ~10.6 km s^{-1}. This is 18% of the shear in the Alfvén velocity (58 km s^{-1}) based on the reconnecting field component B_X. The velocity shear of the transverse (to reconnecting field) velocity ΔV_{pY} was much smaller (2.5 km s^{-1}) in this case.

The second example of a reconnection exhaust in the October 31 ICME is shown in Figures 2(h)–(l). This event has an even larger guide field B_Y (4.2 times the reconnecting field B_X); i.e., the magnetic field rotation angle was only 29°. Because the magnetic shear is so small, the event is nearly unrecognizable on the scale of Figure 2(b), and the magnetic field magnitude is nearly unchanged across the current sheet. The reconnection exhaust is recognized by the proton jetting in the negative X direction (panel (k)), with B_X and V_{pX} being correlated across the left edge and anticorrelated across the right edge of the current sheet. The reduction in the proton radial velocity (panel (l)) inside the current sheet implies that here the X-line was located anti-sunward of *PSP*. The V_{pX} velocity shear (or difference) on the two sides of the current sheet again leads to an asymmetry in the amount of velocity change across the two edges of the current sheet.

The third example (Figures 2(m)–(q)) had larger magnetic shear than the previous two events, and the large rotation of B_X

stands out in Figure 2(b). The |B| reduction inside the current sheet is more visible in this event but is mitigated by the compression of B_Y. However, the magnetic shear was still only 90°, i.e., a guide field of unity. The duration of the current sheet crossing was 7.6 s. This current sheet was located near the compressed trailing edge of the ICME (Figure 2(a)). The reason for the compression appears to be due to the fact that the ICME was moving slower (radially) than the solar wind behind it, a phenomenon that is known to occur frequently in ICMEs at 1 au (e.g., Fenrich & Luhmann 1998; Ruffenach et al. 2015). The event is again characterized by a bifurcated current sheet (sharp changes in B_X at the two edges). The out-of-plane magnetic field B_Y was enhanced inside the current sheet, with small dips at the two edges. Such tripolar B_Y profiles have previously been reported in some solar wind reconnection events (Eriksson et al. 2014, 2015) and in simulations (Eriksson et al. 2015; Zhang et al. 2019). A velocity shear across the current sheet was also present in this event, which again leads to the plateau in B_X being below the half-point of the B_X transition. Finally, the reduction in V_{pR} in the current sheet indicates an anti-sunward location of the X-line relative to *PSP*.

4.2. Reconnection at HCS

Figures 3(a) and (b) show that *PSP* crossed the HCS a number of times during the first orbit, marked by reversals in the B_R component (panel (a)) and the concurrent switching between 0° and 180° pitch angle of fluxes of 320 eV strahl electrons (panel (b)). All of these occurred in regions where SPC had 28 s resolution proton moments; thus, not all current sheets could be resolved by the proton measurements.
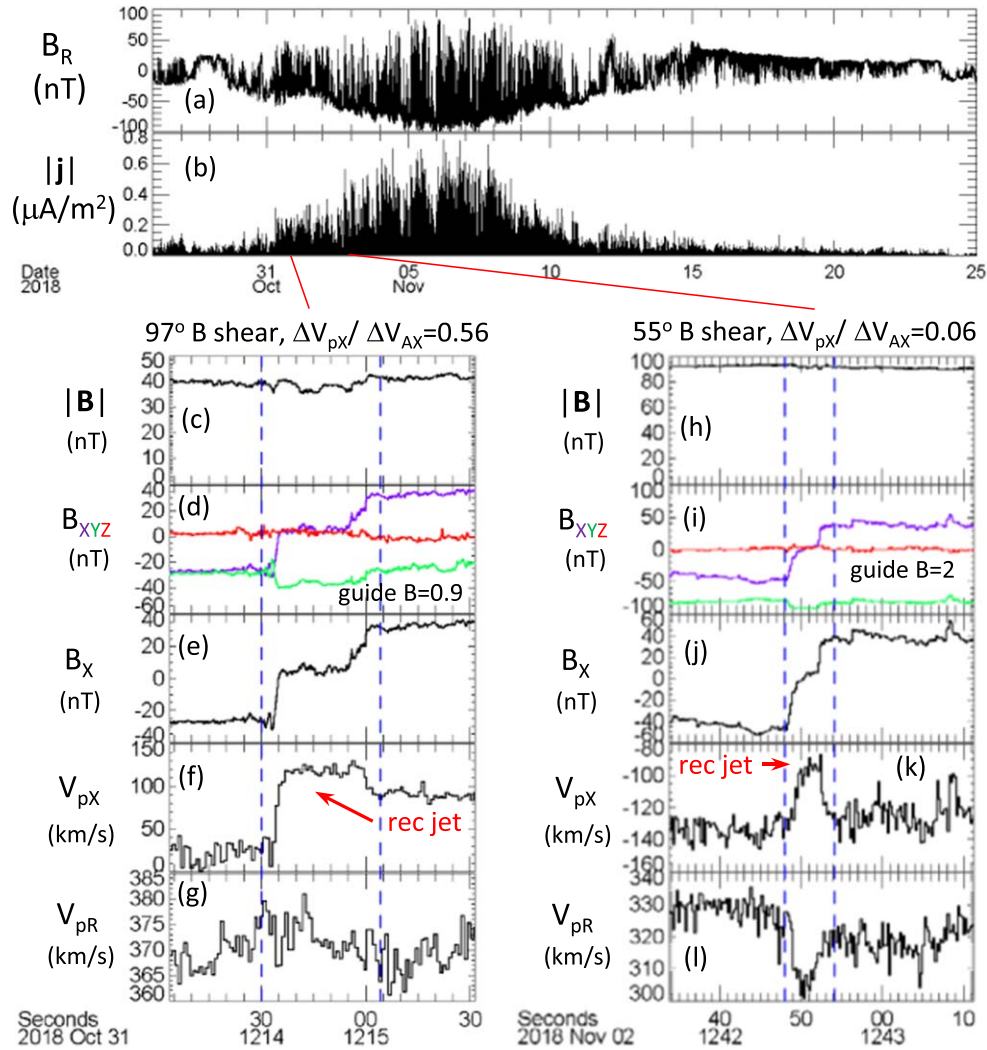
Figure 4. Examples of reconnection exhausts in the regular solar wind. (a) Radial component of the magnetic field. (b) Proxy for current density (see Figure 1 caption). The parameters in panels (c)–(l) are similar to those in Figure 2. The event in panels (h)–(l) illustrates the high quality of 0.22 s resolution SWEAP/SPC proton velocity measurements, which fully resolved the proton reconnection jet in the 5.8 s current sheet crossing.

Nevertheless, we have found possible evidence for reconnection exhausts in the HCS on November 13–15 and 23.

The HCS on November 13–15 seems to be composed of multiple current sheets. Figures 3(c)–(q) display examples of reconnection exhausts in three of the current sheets. All three events had relatively high magnetic shears: 129° (panels (c)–(g)), 168° (panels (h)–(l)), and 108° (panels (m)–(q)). The 168° shear is by far the widest of the three current sheets (see Table 1). It also had a deep $|B|$ minimum (Figure 3(h)), whereas the 129° and 108° events did not. All three events show the presence of accelerated flows consistent with reconnection: opposite δV_{pX}–δB_X correlations at the two edges of the current sheet.

In contrast, the November 23 event (Figures 3(r)–(v)) was a single crossing of the HCS. The crossing occurred at ~107 R_s from the Sun. The magnetic field rotation across the current sheet was 168°; i.e., the magnetic fields on the two sides of the current sheet were nearly antiparallel. There was a deep minimum in $|B|$ in the current sheet (Figure 3(r)), which is a characteristic of high magnetic shear current sheets. Embedded in the current sheet is a proton jet of ~40 km s^{-1} in the X

direction (relative to the external flows), with opposite δV_{pX}–δB_X correlations at the two edges of the current sheet, consistent with reconnection. The enhancement of the radial velocity V_{pR} implies that the X-line was located sunward of PSP. The duration of the HCS crossing was ~11 minutes, which translates to an exhaust width of 1.7×10^5 km, or ~6000 ion inertial lengths.

Interestingly, in these four HCS events, the radial velocity V_{pR} was enhanced as a result of reconnection outflows, which implies that the X-line was sunward of PSP in all cases.

4.3. Reconnection in Regular Solar Wind

In addition to reconnection exhausts occurring in ICMEs and HCS crossings, PSP also detected reconnecting current sheets in the regular solar wind. Figures 4(c)–(l) show two such examples. One event (Figures 4(h)–(l)) was detected when the ion moment resolution was 0.22 s, and the cleanly resolved plasma jet illustrates the quality of this high-resolution data product.

The current sheets in both events were bifurcated (panels (e) and (j)), and plasma jetting was observed in the current sheet
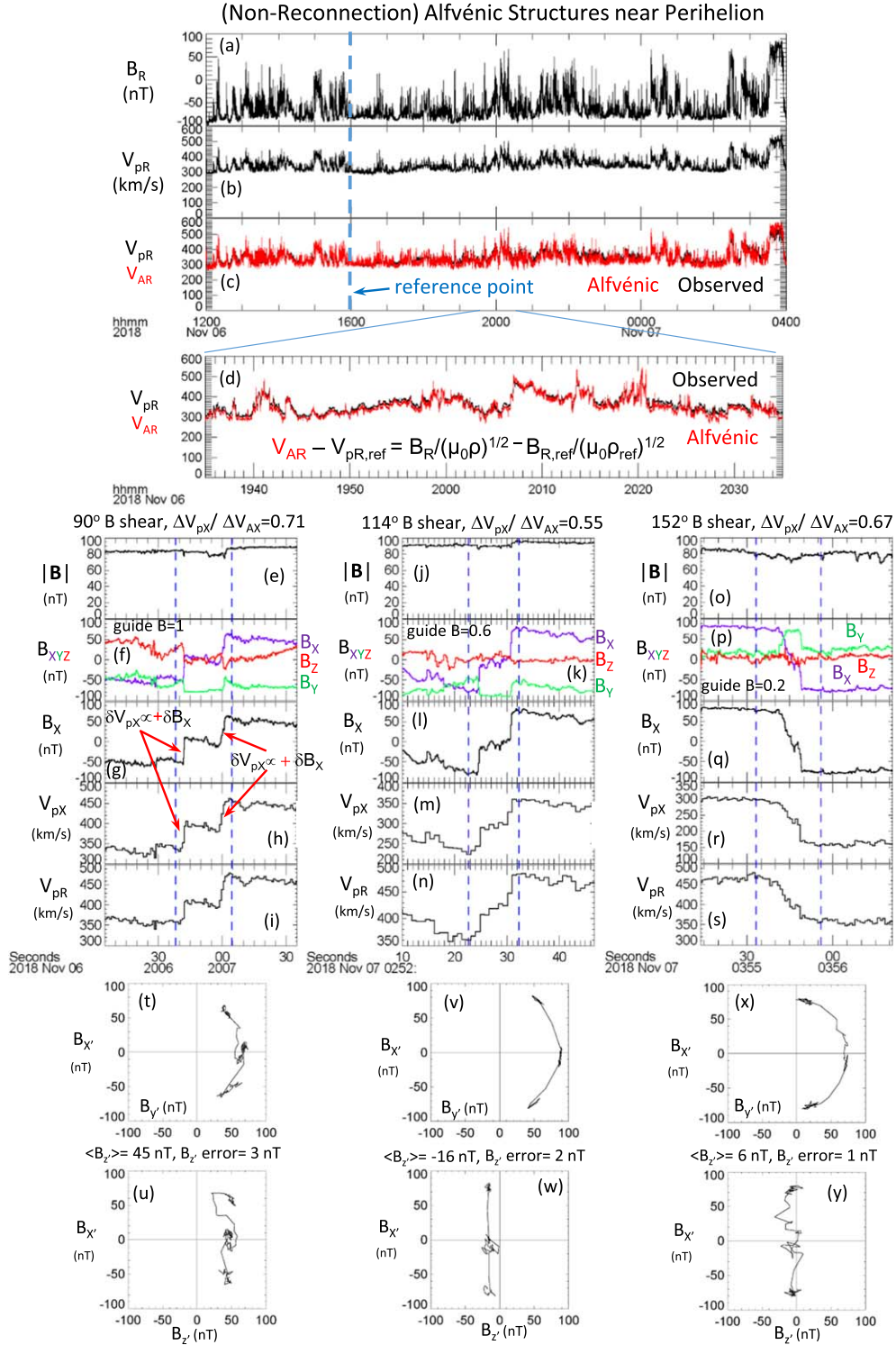
Figure 5. Current sheets close to perihelion are mostly associated with Alfvénic structures rather than reconnection. (a) and (b) Radial component of the magnetic field and ion bulk velocity. (c) Overlaid radial proton velocity and Alfvén velocity. (d) Zoom-in of panel (c). The parameters in panels (e)–(s) are similar to those in Figure 2. Panels (t)–(y) show the magnetic field hodograms in the x'–y' and x'–z' planes determined from MVAB (Section 2). The normal magnetic field errors were estimated using the method by Sonnerup & Scheible (1998). Panels (g) and (h) show how to recognize Alfvénic structures as opposed to reconnection: V_{pX} and B_X variations are positively correlated at both edges of the current sheet. This single (positive) correlation between V_{pR} and V_{AR} persisted throughout the 16 hr interval, indicating that V_{pR} enhancements (from a baseline of $\sim$300 km s^{-1}) are Alfvénic structures, not reconnection jets.

(panels (f) and (k)), with opposite δV_{pX}–δB_X correlations at the two edges of the current sheets (panels (e) and (f) and panels (j) and (k)). Again, because of the relatively large guide field, $|\boldsymbol{B}|$ did not have a deep minimum in these reconnecting current sheets.

4.4. Summary of Reconnection Exhaust Observations

The above examples and additional examples in Table 1 illustrate that reconnection exhausts occur in a variety of solar wind phenomena that *PSP* encountered. They also illustrate the

8

Table 1
List of Reconnection Events

Event No.	Start Time[a] (UT)	Dur.[b] (s)	Width (km)	Width (d_i)	Distance to X-line (R_S)	Magnetic Shear (deg)	Guide Field (nT)	$\Delta V_{pX}/\Delta V_{AX}$	$\Delta V_{pY}/\Delta V_{AX}$	V_R in Reconnection[c]	Distance to Sun (R_s)	Context
1	2018 Oct 27/04:42:00	51.9	4034	198	0.029	133	0.44	0.10	0.079	↑	74.49	SW
2	2018 Oct 29/19:07:30	38.4	7729	422	0.056	120	0.58	0.30	0.062	?	62.01	SW
3	2018 Oct 31/03:38:03	1.60	405	24	0.0029	49	2.2	0.0043	0.19	?	55.42	ICME
4	2018 Oct 31/06:43:20	5.71	1419	88	0.010	35	3.2	0.18	0.043	↑	54.80	ICME
5	2018 Oct 31/07:18:50	6.29	1718	97	0.012	27	4.2	0.21	0.045	↓	54.68	ICME
6	2018 Oct 31/08:31:03	7.61	2143	139	0.015	89	1.0	0.38	0.33	↓	54.44	ICME
7	2018 Oct 31/12:14:30	32.4	3481	183	0.025	97	0.89	0.56	0.35	↑	53.70	SW
8	2018 Oct 31/14:54:32	5.60	1128	70	0.0081	128	0.48	0.34	0.23	↓	53.17	SW
9	2018 Oct 31/14:57:10	4.11	969	51	0.0070	74	1.3	0.39	0.17	↓	53.16	SW
10	2018 Nov 1/08:53:33	2.01	320	20	0.0023	88	1.0	0.24	0.012	↓	49.64	SW
11	2018 Nov 1/23:23:07	3.85	473	31	0.0034	53	2.0	0.047	0.28	↑	46.91	SW
12	2018 Nov 1/23:25:03	27.8	2596	174	0.019	60	1.7	0.13	0.34	↓	46.90	SW
13	2018 Nov 2/12:42:45	5.80	1626	104	0.012	55	1.9	0.064	0.13	↓	44.52	SW
14	2018 Nov 2/13:15:00	7.33	1584	98	0.011	83	1.1	0.26	0.063	↓	44.42	SW
15	2018 Nov 11/23:17:00	65.7	24642	1480	0.18	101	0.82	0.067	0.51	↑	54.62	ICME
16	2018 Nov 13/07:11:00	28.4	3139	170	0.023	129	0.48	0.36	0.11	↑	61.07	HCS
17	2018 Nov 13/10:17:00	42.6	12852	800	0.092	71	1.4	0.48	0.13	↓	61.71	HCS
18	2018 Nov 13/16:15:00	1150	287940	17415	2.1	168	0.11	0.41	0.0039	↑	62.92	HCS
19	2018 Nov 13/23:07:00	14.1	4466	296	0.032	133	0.43	0.29	0.049	↑	64.30	HCS
20	2018 Nov 14/13:20:00	192.0	30687	1694	0.22	108	0.73	0.087	0.28	↑	67.18	HCS
21	2018 Nov 23/18:26:00	650.0	171767	5965	1.2	168	0.10	0.072	0.17	↑	107.20	HCS

Notes.
[a] Left edge of current sheet.
[b] Current sheet crossing duration.
[c] Radial velocity in reconnection exhaust: enhanced (↑), reduced (↓), or ambiguous (?).

various conditions (e.g., magnetic and velocity shears) under which reconnection occurs. Finally, the plasma and field profiles across reconnecting current sheets are dependent on the guide field and velocity shear. Here we summarize some key observations.

1. There is a large range of magnetic shear associated with reconnecting current sheets detected by *PSP*, ranging from $27°$ to $168°$, with a median of $89°$. The largest shears were at HCSs.
2. Only the largest magnetic shear events displayed deep minima in $|\boldsymbol{B}|$.
3. The majority of reconnecting current sheets are bifurcated. However, as will be shown in the next section, bifurcated current sheets do not necessarily imply reconnection.
4. The presence of velocity shear across the current sheet ΔV_{pX} (in the flow component parallel to the reconnecting field) creates an asymmetry in the level of plasma acceleration at the two edges of the current sheet.
5. Approximately half of the reconnection events resulted in enhanced radial velocity V_{pR}, while the others showed reduced V_{pR}. This is consistent with reconnection occurring in the local current sheet, such that statistically, there is an equal chance for *PSP* to be on either side of the *X*-line.
6. The distance from *PSP* to the reconnection site along the outflow direction (X) can be roughly estimated as $(W/2)/R_{\rm rec}$, where W is the width of the exhaust (along *Z*) at *PSP*, and $R_{\rm rec}$ is the dimensionless reconnection rate. Table 1 shows the estimated distance using the canonical reconnection rate of 0.1 (e.g., Birn et al. 2001). The distances to the *X*-line were large for the two main HCSs (up to $2\,R_s$) but much smaller for other events.
7. Many reconnecting current sheets were thin (with a crossing duration $\ll 1$ minute). Adequately resolving such current sheets requires high time resolution (subsecond) plasma and field measurements.

5. Nonreconnecting Current Sheets Associated with Radial Jets and Radial Magnetic Field Switchbacks Near Perihelion

Table 1 lists the reconnection events that we have been able to identify in encounter 1 data so far. It is noted that there are no events found in the interval between 2018 November 2/13:05:07 and 2018 November 11/23:17:00 UT, which encompasses perihelion. This is surprising, because this is the interval with the strongest magnetic fields (Figure 1(a)), largest Alfvén speeds (Figure 1(d)), and current sheets with the highest levels of current density (Figure 1(e)) of orbit 1. Furthermore, high-resolution ($\leqslant 0.9$ s) plasma and ($\ll 0.2$ s) magnetic field data were available throughout the interval; thus, the lack of reconnection events found cannot be attributed to measurement limitations. This interval is dominated by the presence of radial magnetic field polarity changes (termed "switchbacks"; Bale et al. 2019) and spiky plasma jets (Horbury et al. 2020; Kasper et al. 2019). We will focus on a representative interval to illustrate the structures of the plasma and magnetic field and the method used to deduce the absence of reconnection in the local current sheets.

Figures 5(a)–(c) show the radial field and proton radial velocity in a 16 hr interval. It appears that the radial velocity V_{pR} had a baseline velocity of $\sim 300\,{\rm km\,s^{-1}}$, from which the velocity spiked

upward, with enhancements reaching $>200\,{\rm km\,s^{-1}}$ from the baseline. The presence of such jets in a region full of current sheets at first suggests that they could be due to reconnection in the local current sheets. However, the simple fact that the jets were always radially enhanced immediately calls this hypothesis into question. If the jets were due to local reconnection, statistically, one would expect roughly half to be radially decelerated, since there would be an equal chance of *PSP* being on either side of the *X*-line, as is the case for the reconnection events in Table 1.

Another way to determine whether the radial jets are associated with local reconnection or not is to examine the correlation between the variations of B_R and V_{pR} (see Section 2). Figures 5(a) and (b) show that B_R and V_{pR} appear to be positively correlated throughout the 16 hr interval. To assess the degree of Alfvénicity of the velocity variations more precisely, Figures 5(c) and (d) show the observed flows (black) and the predicted radial velocity if it were Alfvénic (red). The predicted velocity is computed based on a single reference time (2018 November 6/16:00 UT), marked by the vertical dashed line in panels (a)–(c). The flow prediction is based on the local magnetic field measurements and the reference velocity and field values: $V_{AR,{\rm predicted}} - V_{pR,{\rm ref}} = +[B_R(\mu\rho)^{-1/2} - B_{R,{\rm ref}}(\mu\rho_{\rm ref})^{-1/2}]$ (Hudson 1970; Paschmann et al. 1986). The positive sign was chosen based on the observed positive correlation between the variations of V_{pR} and B_R in this interval. The subscript "ref" denotes the reference time. The pressure anisotropy effects are omitted for simplicity in the Alfvénic flow prediction.

The agreement between the Alfvén velocity and observed flows is remarkable (Figures 5(c) and (d)), even for flow variations that are hours away from the reference time. The single (positive) correlation between the variations of V_{AR} and V_{pR} throughout the 16 hr interval indicates that the V_{pR} enhancements (from a baseline of $\sim 300\,{\rm km\,s^{-1}}$) are related to Alfvénic structures, not locally generated reconnection jets bounded by pairs of Alfvénic discontinuities (or RDs) propagating in opposite directions along folded magnetic field lines. The positive correlation persisted for days in regions where the large-scale radial field B_R was negative. Interestingly, the single correlation between V_{AR} and V_{pR} suggests that the plasmas in this entire interval were magnetically interconnected; i.e., there were no topological boundaries between them.

The V_{AR}–V_{pR} correlation becomes negative when the large-scale B_R is positive (not shown). Thus, the current sheets near perihelion are Alfvénic structures propagating away from the Sun (Bale et al. 2019; Horbury et al. 2020; Kasper et al. 2019).

To examine the current sheets in Alfvénic structures in more detail, Figures 5(e)–(s) show three examples of individual current sheets viewed in the current sheet *XYZ* coordinate system. In all three examples, the current sheet was bifurcated, with sharp changes in B_X at the two edges of the current sheet. The guide field $|B_Y|$ was enhanced in each of the current sheets. These are common magnetic field profiles in reconnecting current sheets (see Figures 2–4). However, there was no reconnection plasma jetting inside these current sheets: V_{pX} and B_X variations were positively correlated at both edges and all the way through each of the current sheets. Such correlations are predicted for a single RD (as opposed to reconnection back-to-back RDs; see Section 2.2) and are the signature of an Alfvénic structure rather than reconnection. Thus, signatures in the solar wind magnetic field data alone (e.g., current sheet bifurcation) cannot be used to determine the presence or absence of reconnection.

Figures 5(t)–(y) show the magnetic field hodograms of the transitions across the current sheets in the x'–y' and x'–z' planes determined from MVAB (Section 2). The magnetic field structure in the current sheet of the three events is characteristic of RD, with near-circular field rotation in the x'–y' plane and a finite normal magnetic field $B_{z'}$ (Sonnerup & Ledley 1974). The Alfvénic nature of the magnetic field and velocity variations across these current sheets provides further support for the interpretation that these current sheets are RDs (e.g., Paschmann et al. 2013b).

6. Statistical Properties of Reconnection versus Alfvénic Events

To investigate the differences between reconnecting current sheets and Alfvénic structures, we compare the conditions associated with the 21 reconnection exhausts described in Section 4 to those associated with the Alfvénic structures discussed in Section 5.

Given the very large number of current sheets associated with Alfvénic structures near perihelion (Horbury et al. 2020), we limit the survey to a representative 16 hr interval shown in Figures 5(a)–(c) and select a subset of "clean" current sheets that satisfy the following criteria.

1. The current sheet is well defined, with monotonic or near-monotonic rotation of the magnetic field from one side to the other.
2. The external boundary conditions are relatively stable.
3. The radial magnetic field reverses polarity across the current sheet. We chose this condition mainly because it is well defined and limits the number of events. As is shown in Figure 6(a), even with this criterion, we still have a significant number of low magnetic shear events (down to 38°).
4. The current sheet crossing duration is $\geqslant$1.8 s, to allow for at least two plasma measurements inside the current sheet. This is to ensure that the absence of a reconnection jet is not due to measurement resolution limitation.

After applying these criteria, we were left with 43 events. We analyzed all current sheets following the same procedure as described in Section 4 and examined some key parameters that may control the occurrence of reconnection to see what may distinguish the reconnection from the nonreconnection events. These parameters are the magnetic shear angle, β-magnetic shear condition for reconnection, velocity shears, and current sheet thickness.

Figure 6 shows the conditions associated with Alfvénic (nonreconnection; left column) versus reconnecting current sheets detected by *PSP* (middle column). For comparison, we also examined a previously published large data set of 197 reconnection exhausts detected by *Wind* at 1 au (right column; Phan et al. 2010).

6.1. Magnetic Shear Angle

Figures 6(a)–(c) shows no systematic difference in terms of the magnetic shear across the current sheets. The magnetic shear spans a large (mostly in the 20°–150°) range in both reconnection and nonreconnection categories.

6.2. Plasma β-magnetic Shear Condition for the Suppression of Reconnection

Swisdak et al. (2003, 2010), based on kinetic simulations, predicted that the occurrence of reconnection in a current sheet depends on a combination of the difference in the β on the two sides of the current sheet and the magnetic shear angle, θ, across the current sheet. The underlying physics is related to the diamagnetic drift of the X-line associated with the plasma pressure gradient across the current sheet. Reconnection is deemed to be suppressed if the X-line drift speed along the reconnection outflow (X) direction exceeds the reconnection outflow speed. For a given θ, Swisdak et al. (2010) predicted that reconnection is suppressed if $\Delta\beta$ satisfies the relation

$$\Delta\beta > 2(L/\lambda_i)\tan(\theta/2), \qquad (2)$$

where L/λ_i is the width of the plasma pressure gradient layer across the current sheet (near the X-line) in units of the ion skin depth λ_i. This width is a free parameter but is expected to be comparable to the width of the ion diffusion region, which, in turn, is expected to be of the order of λ_i. According to this prediction, reconnection is allowed for a large range of θ at low $\Delta\beta$ but requires large θ at high $\Delta\beta$ values. Thus, it would be easier for reconnection to occur in low β environments, since $\Delta\beta$ would also be small.

Observations of reconnection events in the solar wind at 1 au (Phan et al. 2010; Gosling & Phan 2013) and Earth's magnetopause (Phan et al. 2013; Trenchi et al. 2015) seem to be in agreement with this prediction: for low $\Delta\beta$, reconnection exhausts were observed for a large range of θ, whereas for large $\Delta\beta$, reconnection occurred only when θ was large. This prediction has also been used to explain the high occurrence rate of reconnection at Mercury's magnetopause (DiBraccio et al. 2013) and the low occurrence rate of reconnection at the equatorial magnetopause at Saturn (Masters et al. 2012).

We now address the $\Delta\beta$ and θ conditions for the *PSP* events with the goal of determining whether the $\Delta\beta$ and θ conditions in the Alfvénic events may be different from the reconnection events. The analysis uses only proton β because *PSP* electron temperature data resolution was not sufficiently high for our events. However, based on the *Wind* spacecraft database of 197 reconnection exhausts at 1 au (Phan et al. 2010), $\Delta\beta_{\text{electron}}$ is somewhat correlated with $\Delta\beta_{\text{proton}}$ and comparable in size (not shown). Thus, the true $\Delta\beta$ is likely to be larger (but likely less than a factor of 2) than $\Delta\beta_{\text{proton}}$. This should be kept in mind as one interprets the results in Figures 6(d)–(f).

Figures 6(d)–(f) show that, with the exception of one *PSP* reconnection event (Figure 6(e)), no other reconnection or nonreconnection events were in the parameter regime where reconnection is predicted to be suppressed (below the relation 2 curve in Figures 6(d)–(f)). In fact, the Alfvénic (nonreconnection) events have even smaller $\Delta\beta_{\text{proton}}$ on average than the reconnection events, thus safely away from the marginal diamagnetic drift suppression condition. The smaller $\Delta\beta_{\text{proton}}$ of the Alfvénic events is due to fact that these current sheets were in the lower β region near perihelion. This finding thus reveals that the $\Delta\beta$–θ condition is not a distinguishing factor between reconnection and nonreconnection *PSP* events. It further demonstrates that the $\Delta\beta$–θ reconnection suppression
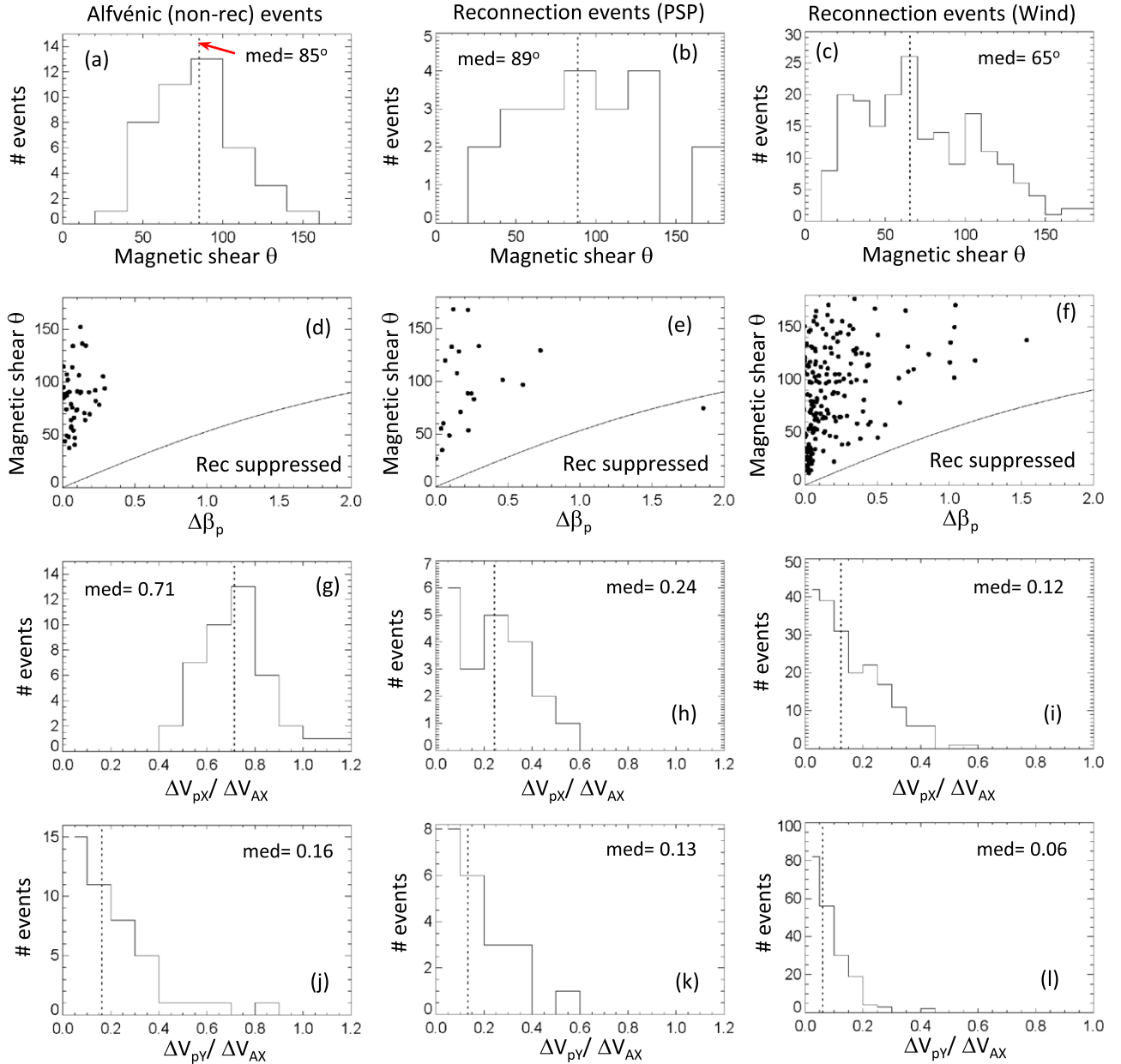
Figure 6. Statistical properties of 43 *PSP* nonreconnecting (Alfvénic) current sheets associated with B_R polarity reversals in the 16 hr interval of panels (a)–(c) (left column), 21 reconnecting current sheets found in *PSP* encounter 1 (middle column), and 197 *Wind* reconnecting current sheets from Phan et al. (2010; right column). (a)–(c) Magnetic shear angle; (d)–(f) difference in proton β across the current sheet vs. θ; (g)–(i) velocity shear across the current sheets in the *X* direction, normalized to Alfvén velocity shear in same direction; and (j)–(l) velocity shear across the current sheets in the out-of-plane *Y* direction, normalized to Alfvén velocity shear in the *X* direction. The solid curve in panels (d)–(f) is the diamagnetic drift suppression marginal condition $\Delta\beta = 2\tan(\theta/2)$, below which reconnection is predicted to be suppressed (Swisdak et al. 2003, 2010). All of the Alfvénic events are in the area above the curve (panel (d)); thus, the lack of reconnection in Alfvénic current sheets is not due to the diamagnetic drift suppression effect. The main noted difference between reconnection (panels (h) and (i)) and nonreconnection (panel (g)) events is the higher velocity shears (in *X*) across Alfvénic (nonreconnecting) current sheets.

condition is a necessary but not sufficient condition for reconnection.

6.3. Velocity Shears

Theories and simulations have predicted that large tangential velocity shears across current sheets exceeding the Alfvén speed can suppress reconnection (e.g., Cowley & Owen 1989; Cassak & Otto 2011). However, as far as we know, the suppression of reconnection by velocity shear has not been demonstrated experimentally. Furthermore, most (if not all) of the theoretical predictions are for the case of a zero or small guide field, whereas in the events examined here, there is often a substantial guide field.

We have examined whether the size of the tangential velocity shear may be different for reconnection and nonreconnection events. Figures 6(g)–(i) show the distributions of the shear in the velocity component parallel to the reconnecting field normalized to the shear of the Alfvén velocity based on the reconnecting field, $\Delta V_{pX}/\Delta V_{AX}$. The general finding is that the Alfvénic (non-reconnection) events have much larger velocity shear than the reconnection events, with a median of 0.71, as opposed to 0.24 and 0.12 for the *PSP* and *Wind* reconnection events, respectively.

This may suggest that local reconnection was suppressed for large (but sub-Alfvénic) velocity shears. We note that the observed velocity shear almost never exceeded unity; i.e., boundary conditions with velocity shears larger than the Alfvén velocity shear do not seem to exist in this solar wind (Figure 6(g)).

While MHD-based theories have predicted (for antiparallel reconnection with no guide field) the suppression of reconnection to occur when the normalized velocity shear exceeds unity (e.g., Cassak & Otto 2011), these predictions are related to the reconnection outflow being at the Alfvén speed. However, in observations (including those of *PSP* described in Section 4.1), as well as in kinetic simulations, the outflow jet speed is generally sub-Alfvénic (e.g., Paschmann et al. 1986; Øieroset et al. 2000; Haggerty et al. 2018). If the reconnection outflow is sub-Alfvénic, it seems possible that reconnection could be suppressed at a velocity shear that is sub-Alfvénic.

We also examined the normalized shear of the transverse velocity component $\Delta V_{pY}/\Delta V_{AX}$ and found no significant difference between the reconnection and nonreconnection events, and ΔV_{pY} was much smaller than ΔV_{pX} in general.

Another possible explanation for the different velocity shears for the reconnection and Alfvénic events is that current sheets that reconnect are those that were originally TDs (with velocity shears that are unrelated to the local Alfvén speed), whereas the current sheets in Alfvénic structures are RDs, which contain finite normal magnetic fields and Alfvénic velocity shears. There are presumably plasma flows through RDs as well, which are usually not measurable. RDs are not known to reconnect.

6.4. Current Sheet Thickness

As shown in Table 1, *PSP* reconnection events exhibit a large range of current sheet crossing durations and thicknesses, ranging from 1.6 s (24 ion inertial length d_i) to 1150 s (17,415 d_i), with a median of 14 s (170 d_i), where the thickness is the product of the crossing duration and the average normal velocity V_{pZ} measured at the two edges of the current sheet. For the 43 Alfvénic (nonreconnection) events that we studied, the median current sheet crossing duration and width were smaller, 7.5 s (90 d_i), and the width ranges from 9 to 455 d_i.

In collisionless reconnection, it is generally understood that reconnection is triggered only when the thickness of a current sheet is of the order of an ion inertial length or smaller (e.g., Sanny et al. 1994). Thus, it seems that all of the (reconnecting and nonreconnecting) current sheets we examined were too thick to reconnect. However, for reconnection events, the relevant current sheet thickness for triggering reconnection is around the *X*-line. After reconnection is triggered, the exhaust widens with increasing distance from the *X*-line, and *PSP* generally crosses the exhaust at some distance downstream of the *X*-line. On the other hand, the thicker-than-d_i-scale Alfvénic current sheets may still be a factor in stabilizing reconnection.

7. Summary and Discussions

During the first orbit, *PSP* encountered reconnection exhausts in ICMEs, HCS crossings, and the regular solar wind. Many of the reconnecting current sheets were bifurcated, resembling Petscheck's model of reconnection with a pair of slow-shock/RD-like structures bounding the exhaust (Petscheck 1964; Lin & Lee 1993). All of the reconnection exhausts identified so far in orbit 1 were detected relatively far from the Sun (44.4–107.2 R_s).

About half of the reconnection events had a magnetic shear $<90°$, and one case had a magnetic shear of $27°$, i.e., a guide field of 4. The extreme low shear current sheets produced plasma jetting as slow as $10 \, \mathrm{km \, s^{-1}}$ (relative to the external flows). The well-resolved current sheets with clean plasma and field signatures of reconnection clearly demonstrated the capability of *PSP* to detect reconnection exhausts in the solar wind.

Magnetic reconnection in ICMEs is important, as it can cause erosion and changes to the magnetic field structure that may be relevant for understanding their geoeffectiveness at Earth (e.g., Fermo et al. 2014; Lavraud et al. 2014). The *PSP* measurements presented here show that reconnection within ICMEs can, in fact, already be operating at 54–55 R_S from the Sun, which means reconnection could work to affect the ICME structure for the majority of its transit from the Sun to 1 au. Similarly, the detection of well-established reconnection exhausts in the HCS observed inside of 61 R_s indicates that magnetic topology around the HCS is already being altered at relatively close distances to the Sun.

Surprisingly, however, we were not able to find reconnection exhausts during the 9 days (2018 November 2/13:15–2018 November 11/03:28 UT) around perihelion, even though this period had the highest Alfvén speed and lowest plasma β of orbit 1. The perihelion period was dominated by Alfvénic structures associated with bursty radial jets that may have originated from a coronal hole (Bale et al. 2019; Badman et al. 2020). Similar Alfvénic structures (or pulses) have previously been detected by the *Helios* spacecraft further away from the Sun, at $\sim$60 R_s (Horbury et al. 2018) and 1 au (Gosling et al. 2011; Matteini et al. 2014). None of the current sheets associated with these Alfvénic structures that we have examined appear to be undergoing local reconnection at the *PSP* location.

To identify the possible conditions that may control the onset of local reconnection, we compared the plasma and field conditions surrounding current sheets with and without reconnection. The main noticeable difference is the degree of tangential plasma flow shear relative to the Alfvén velocity shear, $\Delta V_{pX}/\Delta V_{AX}$, with Alfvénic events having much larger velocity shear than reconnection events. Our finding may suggest that large but sub-Alfvénic velocity shears could suppress reconnection.

An alternative explanation for the absence of reconnection in the Alfvénic current sheets is that these current sheets are RDs (see Section 5). We postulate that, in addition to near-Alfvénic flow shears, the finite normal magnetic field (Buechner & Zelenyi 1987) and associated normal plasma flow (at the Alfvén speed based on the normal magnetic field) through the RDs could preclude these current sheets from reconnecting locally. The thicker-than-d_i-scale Alfvénic current sheets may also be a factor in stabilizing reconnection. If and how reconnection can be triggered in RDs will need to be investigated in future studies.

It is presently not clear why most of the current sheets near orbit 1 perihelion are Alfvénic (or RD) in nature. From just one *PSP* pass, we are not able to determine whether the observed lack of local reconnection in current sheets near perihelion is a general phenomenon or a one-time occurrence associated with the specific solar wind encountered during orbit 1. In principle, the low-β, high Alfvén speed environment close to the Sun is expected to be more favorable to the onset of reconnection than the solar wind farther away. Intercomparison of data from

future *PSP* orbits sampling different types of solar wind will shed further light on this matter.

ORCID iDs

S. D. Bale ⓘ https://orcid.org/0000-0002-1989-3596
J. P. Eastwood ⓘ https://orcid.org/0000-0003-4733-8319
B. Lavraud ⓘ https://orcid.org/0000-0001-6807-8494
J. F. Drake ⓘ https://orcid.org/0000-0002-9150-1841
M. A. Shay ⓘ https://orcid.org/0000-0003-1861-4767
M. Pulupa ⓘ https://orcid.org/0000-0002-1573-7457
M. Stevens ⓘ https://orcid.org/0000-0002-7728-0085
R. J. MacDowall ⓘ https://orcid.org/0000-0003-3112-4201
A. W. Case ⓘ https://orcid.org/0000-0002-3520-4041
J. Kasper ⓘ https://orcid.org/0000-0002-7077-930X
A. Szabo ⓘ https://orcid.org/0000-0003-3255-9071
K. E. Korreck ⓘ https://orcid.org/0000-0001-6095-2490
T. Dudok de Wit ⓘ https://orcid.org/0000-0002-4401-0943
D. Malaspina ⓘ https://orcid.org/0000-0003-1191-1558
M. Velli ⓘ https://orcid.org/0000-0002-2381-3106

References

Abdo, A. A., Ackermann, M., Ajello, M., et al. 2011, Sci, 331, 739
Antiochos, S., DeVore, C. R., & Klimchuk, J. A. 1999, ApJ, 510, 485
Babcock, H. W. 1961, ApJ, 133, 572
Badman, S. T., Bale, S. D., & Martínez Oliveros, J. C. 2020, ApJS, doi:10.3847/1538-4365/ab4da7
Bale, S. D., Badman, S. D., Bonnell, J. W., et al. 2019, Natur, 573, 237
Bale, S. D., Goetz, K., Harvey, P. R., et al. 2016, SSRv, 204, 49
Birn, J., Drake, J. F., Shay, M. A., et al. 2001, JGR, 106, 3715
Buechner, J., & Zelenyi, L. M. 1987, JGR, 92, 13456
Case, A., Kasper, J. C., Stevens, M. L., et al. 2020, ApJS, doi:10.3847/4365/ab5a7b
Cassak, P. A., & Otto, A. 2011, PhPl, 18, 074501
Cowley, S. W. H., & Owen, C. J. 1989, P&SS, 37, 1461
Davis, M. S., Gosling, J. T., & Skoug, R. M. 2006, GeoRL, 33, L19102
DiBraccio, G. A., Slavin, G. A., Boardsen, S. A., et al. 2013, JGR, 118, 997
Duncan, R., & Thompson, C. 1992, ApJL, 392, L9
Dungey, J. W. 1961, PhRvL, 6, 47
Eriksson, S., Gosling, J. T., Phan, T. D., et al. 2009, JGR, 114, A07103
Eriksson, S., Lapenta, G., Newman, D. L., et al. 2015, ApJ, 805, 43
Eriksson, S., Newman, D. L., Lapenta, G., & Angelopoulos, V. 2014, PPCF, 56, 064008
Fenrich, F. R., & Luhmann, J. G. 1998, GeoRL, 25, 2999
Fermo, R. L., Opher, M., & Drake, J. F. 2014, PhRvL, 113, 031101
Fox, N. J., & McComas, D. J. 2016, SSRv, 204, 1
Giovanelli, R. G. 1946, Natur, 158, 81
Gosling, J. T. 2007, ApJL, 671, L73
Gosling, J. T., Eriksson, S., Skoug, R. M., McComas, D. J., & Forsyth, R. J. 2006b, ApJ, 644, 613
Gosling, J. T., McComas, D. J., Skoug, R. M., & Smith, C. W. 2006a, GeoRL, 33, L17102
Gosling, J. T., & Phan, T. D. 2013, ApJL, 763, L39
Gosling, J. T., Phan, T. D., Lin, R. P., & Szabo, A. 2007, GeoRL, 34, L15110
Gosling, J. T., Skoug, R. M., McComas, D. J., & Smith, C. W. 2005a, JGRA, 110, A01107
Gosling, J. T., Skoug, R. M., McComas, D. J., & Smith, C. W. 2005b, GeoRL, 32, L05105
Gosling, J. T., & Szabo, A. 2008, JGR, 113, A10103
Gosling, J. T., Tian, H., & Phan, T. D. 2011, ApJL, 737, 35
Haggerty, C. C., Shay, M. A., Chasapis, A., et al. 2018, PhPl, 25, 102120
Hapgood, M. A. 1992, P&SS, 40, 711
Horbury, T. S., Matteini, L., & Stansby, D. 2018, MNRAS, 478, 1980
Horbury, T. S., Woolley, T., Laker, R., et al. 2020, ApJS, doi:10.3847/1538-4365/ab5b15
Hudson, P. D. 1970, P&SS, 18, 1611
Hurley, K., Boggs, S. E., Smith, D. M., et al. 2005, Natur, 434, 1098
Kasper, J. C., Abiad, R., Austin, G., et al. 2016, SSRv, 204, 131
Kasper, J. C., Bale, S. D., Belcher, J. W., et al. 2019, Natur, 576, 228
Klimchuck, J. A. 2006, SoPh, 234, 41
Korreck, K., Szabo, A., Nieves-Chinchilla, T., et al. 2019, ApJS, submitted
Kronberg, P. P. 2002, PhT, 55, 40
Lavraud, B., Gosling, J. T., Rouillard, A. P., et al. 2009, SoPh, 256, 379
Lavraud, B., Rouillard, A. P., & Owens, M. J. 2011, SoPh, 270, 285
Lavraud, B. A., Ruffenach, A., Rouilldard, A., et al. 2014, JGRA, 119, 26
Leighton, R. B. 1969, ApJ, 140, 1547
Lin, Y., & Lee, L. C. 1993, JGR, 98, 3919
Liu, Y. H., Drake, J. F., & Swisdak, M. 2012, PhPl, 18, 92102
Masters, A., Eastwood, J. P., Swisdak, M., et al. 2012, GeoRL, 39, 8103
Matteini, L., Horbury, T. S., Beugebauer, M., & Goldstein, B. E. 2014, GeoRL, 41, 259
Mistry, R., Eastwood, J. P., Phan, T. D., & Hietala, H. 2015, GeoRL, 42, 10513
Mistry, R., Eastwood, J. P., Phan, T. D., & Hietala, H. 2017, JGRA, 122, 6
Øieroset, M., Phan, T. D., Lin, R. P., & Sonnerup, B. U. O. 2000, JGR, 105, 25247
Owens, M. J., Schwadron, N. A., Crooker, N. U., Hughes, W. J., & Spence, H. E. 2007, GeoRL, 34, L06104
Parker, E. N. 1963, ApJS, 8, 177
Parker, E. N. 1983, ApJ, 264, 642
Parker, E. N. 1988, ApJ, 330, 474
Paschmann, G., Haaland, S., Sonnerup, B. U. O., & Knetter, T. 2013b, AnGeo, 31, 871
Paschmann, G., Oieroset, M., & Phan, T. D. 2013a, SSRv, 178, 385
Paschmann, G., Papamastorakis, I., Baumjohann, W., et al. 1986, JGR, 91, 1271
Petscheck, H. E. 1964, NASSP, 50, 425
Phan, T. D., Gosling, J. T., & Davis, M. S. 2009, GeoRL, 36, L09108
Phan, T. D., Gosling, J. T., Davis, M. S., et al. 2006, Natur, 439, 175
Phan, T. D., Gosling, J. T., Paschmann, G., et al. 2010, ApJL, 719, L199
Phan, T. D., Paschmann, G., Gosling, J. T., et al. 2013, GeoRL, 40, 11
Priest, E. R. 1984, GMS, 30, 63
Ruffenach, A. B., Lavraud, B., Farrugia, C. J., et al. 2015, JGR, 120, 43
Ruffenach, A. B., Lavraud, B., & Owens, M. J., et al. 2012, JGRA, 117, A09101
Sanny, J., McPherron, R. L., Russell, C. T., et al. 1994, JGR, 99, 5805
Slavin, J., & Holzer, R. E. 1979, JGR, 84, 2076
Sonnerup, B. U. Ö., & Cahill, L. J., Jr. 1967, JGR, 96, 171
Sonnerup, B. U. Ö., & Ledley, B. G. 1974, JGR, 79, 4309
Sonnerup, B. U. Ö., Paschmann, G., & Papamastorakis, I. 1981, JGR, 86, 10049
Sonnerup, B. U. Ö., & Scheible, M. 1998, ISSIR, 1, 185
Swisdak, M., Opher, M., Drake, J. F., & Alouani, B. F. 2010, ApJ, 710, 1769
Swisdak, M., Rogers, B. N., Drake, J. F., & Shay, M. A. 2003, JGR, 108, 1218
Szabo, A., Larson, D. E., Whittlesey, P., et al. 2020, ApJS, doi:10.3847/1538-4365/ab5dac
Teh, W. L., Sonnerup, B. U. O., Hu, Q., & Farrugia, C. J. 2009, AnGeo, 27, 807
Trenchi, L., Marcucci, M. F., & Fear, R. C. 2015, GeoRL, 42, 6219
Whittlesey, P., Larson, D. E., Kasper, J. C., et al. 2019, ApJS, submitted
Yamada, M. 2010, RvMP, 82, 603
Zhang, Q., Drake, J. F., & Swisdak, M. 2019, PhPl, 26, 072115